Proceedings of GPPS Forum 18
Global Power and Propulsion Society
Montreal, 7th-9th May 2018
www.gpps.global

GPPS-NA-2018-0005

NUMERICAL SIMULATION OF A MODEL SPRAY FLAME UNDER MILD CONDITIONS USING STOCHASTIC UPSTREAM FLOW AND TEMPERATURE FORCING

Benedict Enderle, Felix Grimm, Georg Eckel, Manfred Aigner
German Aerospace Center (DLR)
benedict.enderle@dlr.de
Stuttgart, Germany

ABSTRACT

Numerical simulations of the Delft Spray in Hot Co-flow (DSHC) flame are presented, in order to aid the understanding of reacting multiphase flows under moderate or low-oxygen dilution (MILD) conditions. The test case consists of a single swirled pressure atomizer installed in the center of a cylindrical hot co-flow, operated with ethanol fuel. A large variety of experimental data is available for the burner's MILD combustion configuration. Here, the particular H-II case is studied.

Three different modelling approaches are employed, an unsteady RANS simulation and two scale-resolving methods, namely LES (Large Eddy Simulation) and SAS-SST (Scale Adaptive Simulation) in combination with a Shear Stress Transport turbulence model. Here, for the scale resolving SAS and LES, transient inflow boundary conditions are necessary in order to propagate turbulent flow and temperature structures into the computational domain, supporting the evolution of a full turbulent energy cascade. However, preliminary simulations have shown that due to the low Reynolds number of the co-flow, artificially imposed spatial and temporal turbulent fluctuations of temperature and velocity field are subject to strong artificial decay, prior to reaching the actual combustion zone.

Therefore, a simplified stochastic forcing approach based on a first order Langevin model is adopted, reducing the boundary condition to a time dependent function which generates time-coherent structures featuring turbulent decay in time. The accurate implementation of the methodology is verified by means of analytical solutions and validated with the Delft Spray flame test case.

INTRODUCTION

Computational simulation of reacting multiphase flows still poses major challenges due to the high computational demands and complex formulation of boundary conditions for both continuous and dispersed phase. However, these simulations can offer detailed insight into the combustion process and aid the understanding of complex combustion processes. In addition, the design process of new combustors increasingly relies on preliminary computational design studies which require accurate and efficient prediction of all aspects of the combustion process in order to meet performance and emission targets.

Moderate or Intense Low-oxygen Dilution (MILD) combustion is seen as a promising technology for the reduction of NO_X emissions. In such a combustion regime, the oxygen stream is diluted by a substantial amount of hot flue gases before reacting with the fuel. This results in a more uniform temperature distribution and lower NO_X emission than in case of conventional combustion (Cavaliere et al., 2004). An extensive range of both experimental and numerical studies on MILD combustion of gaseous fuels is available in the literature (De Joannon et al, 2005; Mancini et al., 2008; Li et al., 2014) but little is reported on spray combustion under MILD conditions. Ye et al (Ye et al., 2015) used prevaporized liquid fuels in their experiments whereas Reddy (Reddy et al., 2014) investigated combustion of liquid kerosene under MILD conditions. Similarities between MILD combustion of gaseous and liquid fuels were found by Weber et al (Weber et al., 2005). Nevertheless, in turbulent spray flames additional phenomena such as droplet dynamics and evaporation come into play requiring comprehensive measurement techniques in order to acquire data on these effects.

Therefore, a simplified laboratory scale burner (DSHC) enabling the use of optical measurement methods was developed to study spray combustion of liquid ethanol under MILD conditions (Rodrigues et al., 2015). In addition to the experiments, numerical studies on the DSHC flame were performed using Reynolds Averaged Navier Stokes Simulation (RANS) in combination with a transported PDF combustion model (Ma et al., 2016a) as well as Large Eddy Simulations (LES) in combination with a non-adiabatic

This work is licensed under a Creative Commons Attribution 4.0 International License CC-BY 4.0

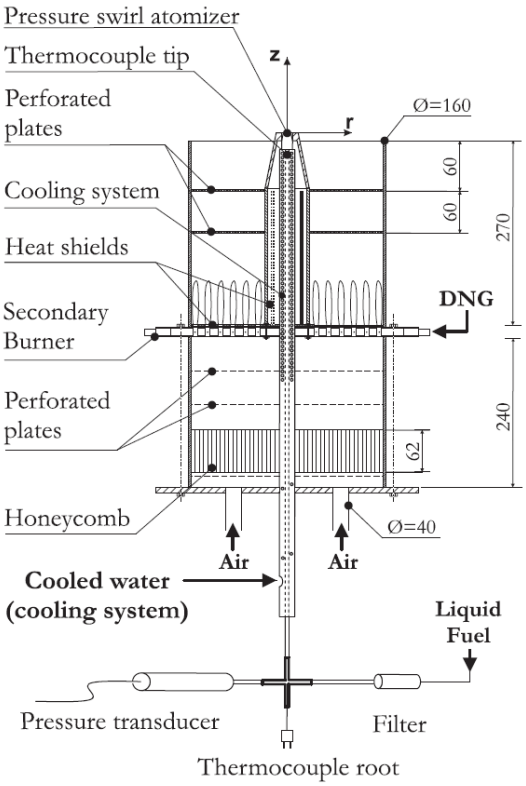

Figure 1 Burner with dimensions in mm.
(Rodrigues et al., 2015)

Flamelet Generated Manifold model (Ma et al., 2016b). LES-pdf results on the same case where reported by Gallot-Lavallee et al (Gallot-Lavallee et al., 2016).

In the present work, simulation methods of different degrees of fidelity in combination with a Finite Rate Chemistry combustion model are compared. While in the unsteady RANS (URANS) approach only unsteady behaviour in the mean quantities is captured, Large Eddy Simulation (LES) aims on resolving a wide range of the turbulent energy cascade. As a third approach, the hybrid URANS-SAS (Scale Adaptive Simulation) model as described by Menter (Menter et al., 2003) is used. In this model, the von Karman length-scale is used to dynamically switch between URANS and LES-like behaviour.

For scale resolving SAS and LES approaches, transient inflow boundary conditions are necessary in order to propagate turbulent flow and temperature structures into the computational domain, supporting the evolution of a full turbulent energy cascade. However, preliminary simulations using a synthetic turbulence generator based on digital filtering as proposed by Klein et al (Klein et al, 2003) have shown that due to the low Reynolds number in the DSHC

Table 1 Co-flow properties after secondary combustion.

$\bar{T}_{cf}[K]$	$\bar{X}_{O2,cf}$	$\bar{X}_{N2,cf}$	$\bar{X}_{H2O,cf}$	$\bar{X}_{CO2,cf}$
1400	0.0871	0.7426	0.1251	0.0634

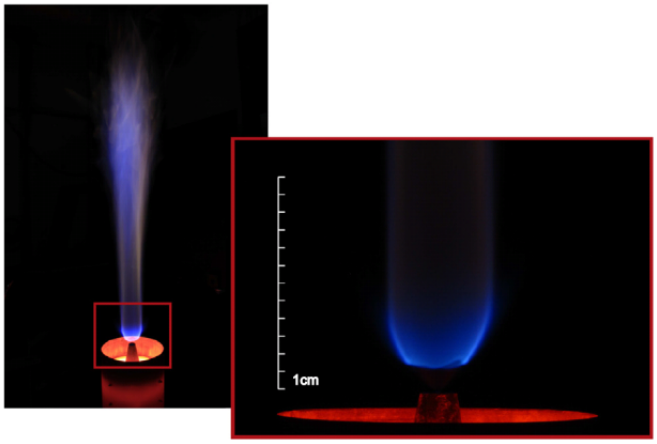

Figure 2 Image of the spray flame with ethanol.
(Rodrigues et al., 2015)

case, artificially imposed spatial and temporal turbulent fluctuations of the temperature and velocity field are subject to strong damping prior to reaching the actual combustion zone. Therefore, a simplified stochastic forcing approach based on a first order Langevin model is analyzed and adopted in this work, reducing the boundary condition to a time dependent function which generates time-coherent structures.

TEST CASE DESCRIPTION

The investigated test case is the Delft Spray in Hot Co-flow flame.

Test Case Specifications

A pressure-swirl atomizer generates a spray of fuel droplets in co-flow of hot combustion products. A schematic of the burner is shown in Fig. 1.

The reference point is set at the tip of the pressure swirl atomizer. A cylinder separates the hot co-flow from the surrounding air. The downstream perforated plates keep the central fuel supply concentric. A secondary burner operated with air and Dutch natural gas (DNG) is fed upstream by air, which is rectified by a honeycomb structure and perforated plates. The hot, diluted co-flow is generated by a matrix burner, consisting of 236 lean flamelets. The DNG molar composition is usually 81.3% methane, 14.4% nitrogen, 3.7% ethane and 0.6% other species (Rodrigues et al., 2015). The spray flame operation at the herein investigated operation point is shown in Fig. 2.

Operation Conditions

The DSHC flame data set consists of multiple operation conditions (Ma et al., 2016c). The present study focuses on the so called HII-case. Ethanol is utilized as fuel and a secondary burner generates the hot combustion co-flow products. The fuel is induced through the spray nozzle with $\dot{m}_{liquid} = 1.46\ kg/h$ at a pressure of $p_f = 11.5\ bar$ and the temperature $T_f = 301\ K$. The spray's characteristic Weber number is $We = 0.46$. The co-flow is fed with upstream air, $\dot{m}_{air} = 51\ kg/h$, resulting in a mean velocity of $\bar{U}_{cf} = 2.5\ m/s$ in combination with $\dot{m}_{DNG} = 2.13\ kg/h$. Properties

of the co-flow composition after the matrix-burner are listed in Table 1.

Measurement Data

Experimental data is available for flow field and combustion, droplet velocity and size statistics, as well as exhaust gas composition (Ma et al., 2016; Rodrigues et al., 2015). In the presented study, velocity and temperature profiles are opposed to numerical simulation data for radial lines at heights of $z = 15{,}20{,}40{,}60mm$, while z denotes the burner centre axis with $z = 0mm$ at the tip of the spray nozzle. Velocity data was measured at those co-flow radial profiles via LDA (Laser Doppler Anemometry) and temperature information was supplied by CARS (Coherent Anti-Stokes Raman Spectroscopy). PDA (Phase Doppler Anemometry) is employed for taking spray characteristics in the spray region. Details on experimental setup and measurement methods can be found in the literature (Ma et al., 2016; Rodrigues et al., 2015).

NUMERICAL SIMULATIONS

As mentioned previously, three different simulation approaches are used and compared to each other in view of reproduction quality of experimental data. All calculations are carried out in the DLR in-house code THETA (Turbulent Heat Release Extension of the TAU Code, (Domenico et al., 2011; Reichling et al., 2013)). For the depiction of liquid phase dynamics, THETA is coupled with SPRAYSIM (Eckel et al., 2016) by means of an online two-way coupling via source terms.

Computational Domain

The computational domain is shown in Fig. 3. The cylindrical domain surrounds the injector with a diameter of $D = 0.3m$ and the height $H = 0.3m$. The spray nozzle is modelled as a discrete point of liquid fuel injection.

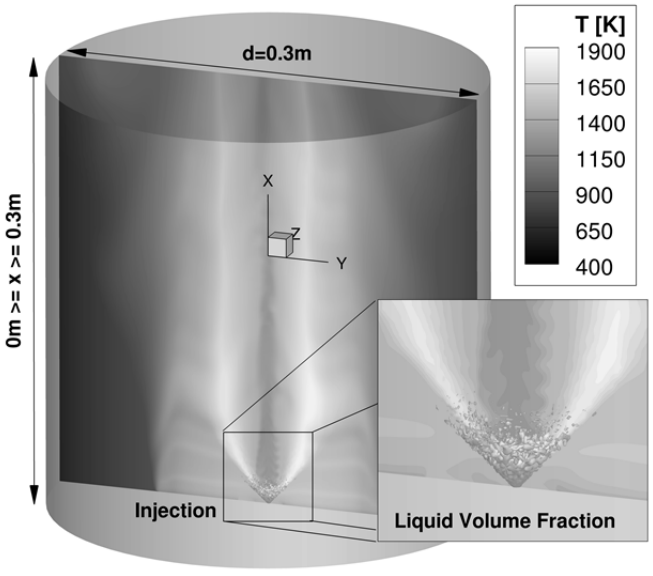

Figure 3 Computational Domain with mid-plane cut of instantaneous temperature distribution and iso-surface of liquid phase volume fraction.

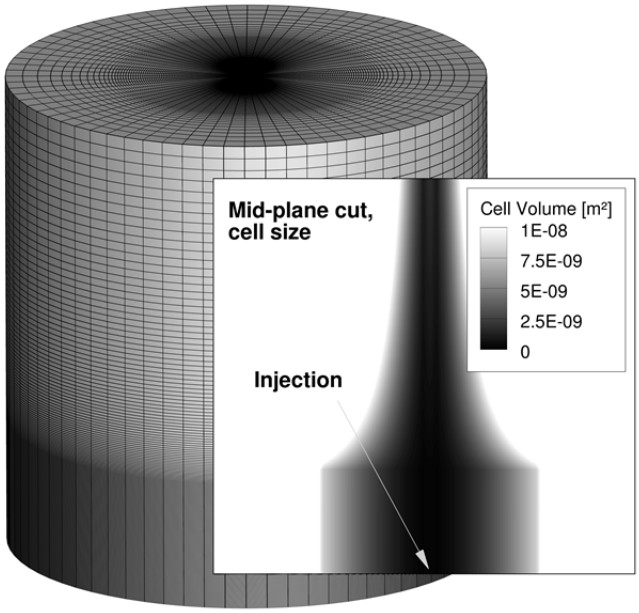

Figure 4 Computational grid size with depiction of cell size.

As can be seen in Fig. 3, the matrix burner producing the hot co-flow is not explicitly modelled but set as velocity inlet. In order to capture temperature fluctuations in the simulation, this boundary is dynamically forced with a stochastic Langevin approach (Pope, 2000). An ambient inflow surrounds the co-flow, also modelled as velocity inlet boundary with $u_{amb} = 0.1\ m/s$. Due to the low outer flow speeds, the cylindrical boundaries are set as symmetries. The downstream circular plane is set as pressure outlet. A small circular disc surrounds the fuel injection, which denotes the leading edge of the fuel nozzle in Fig. 1. The computational grid is fully structured and consists of 1.565 million elements and 1.580 million points. It is shown in Fig. 4, together with a mid-plane distribution of cell size.

For comparison, the URANS is also computed on a

Table 2 Specifications of simulation approaches. Abbreviations are redefined in the nomenclature.

	URANS	***SAS***	***LES***
Turbulence Model	SST	SST	WALE
Time-step	$1e^{-05}s$	$1e^{-05}s$	$1e^{-05}s$
Spatial Discretization	QUDS	CDS	CDS
Time Progression	TPB	TPB	TPB
Chemistry model	FRC	FRC	FRC
Turbulence-Chemistry Interaction	A-PDF	A-PDF	A-PDF
Multigrid	V5+	V5+	V5+

coarse grid with same structure but reduce number of 811.000 elements.

Model Specifications

As mentioned previously, three different simulation approaches are used, compared to each other and validated against experimental data. Those are in particular an URANS (Unsteady Reynolds Averaged Navier Stokes) simulation, and SAS (Scale Adaptive Simulation) and one LES (Large Eddy Simulation). They are consistently performed on the computational grid shown in Fig. 4. Simulation specifications are listed in Table 2.

The combustion of ethanol is described using the detailed reaction mechanism of Roehls and Peters (Roehls and Peters, 2009), incorporating 38 species and 228 reactions.

Molecular heat radiation for CO_2 and H_2O are explicitly considered here, since they are particularly clustered in the reaction zone and therefore highly relevant for depicting the correct temperature distribution.

Turbulence and turbulent temperature fluctuations are poorly resolved in the URANS simulation case. Therefore, an additional transport equation for the determination of temperature standard deviation is taken into account as part of the assumed probability density (A-PDF) turbulence chemistry interaction (TCI) model, reading

$$\bar{\rho}\nabla\cdot\left(\widetilde{T''^2}u\right)-\nabla\cdot\left[\left(\frac{\mu}{Pr}+\frac{\mu_t}{Pr_t}\right)\nabla\widetilde{T''^2}\right]= = 2\frac{\mu_t}{Pr_t}\left(\nabla\tilde{T}\right)^2-\frac{2\bar{\rho}\widetilde{T''^2}}{\tau_T}. \quad (1)$$

$\bar{\rho}$ is the mean density, μ and Pr are the viscosity and the Prandtl number. The indices t and T indicate turbulent and turbulent temperature associated. The $\sim$ denotes Favre averaging. Fluctuations in SAS and LES are directly resolved and sampled. The maximum height of downstream measurement locations is $h = 0.06m$. The length of the computational domain is $H = 5h = 0.3m$. With consideration of the bulk velocity $\bar{U}_{cf}$ this results in a flow-through time of $\tau_H = H/\bar{U}_{cf} = 0.12s$. The flow through time for the measurement region correspondingly amounts to $\tau_h = 0.024s$. Simulations are run for $10\tau_h$, before averaging over $20\tau_h$, while fluctuations are recorded for the last $10\tau_h$.

Liquid Phase Modelling

The liquid phase is computed by SPRAYSIM through a Lagrangian particle tracking method using a point droplet approximation. During one second of simulation time $2\cdot 10^7$particles are injected. Each particle is sampled from a Rosin-Rammler distribution function (Lefebvre, 1998) with $q = 3$ and $X = 45\mu m$. As the atomizer forms a hollow cone spray (Rodrigues et al., 2015), particles are injected with a mean trajectory angle of $\theta = 30°$ augmented by a dispersion angle up to $\theta' = \pm 10°$. Following the findings of Ma (Ma et al., 2016b), the mean absolute velocity of droplets is set to $U_d = 35.7m/s$ and the liquid temperature is set to $T = 301K$.

Evaporation is computed using the vaporization model of Abramzon and Sirignano (Abramzon and Sirignano, 1989). In the URANS and SAS simulations unresolved turbulent droplet dispersion is accounted for by a variant of the Gosman-Ioannides model (Gosman and Ioannides, 1983) while in the LES the model proposed by Bini and Jones is used (Bini and Jones, 2008).

Stochastic Inlet Forcing

One of the main issues with simulating the HII-case of the Delft Spray in Hot Co-flow flame is the correct depiction of temperature RMS levels in the combustion region, which are directly correlated with the upstream matrix burner, as shown in Fig. 1. In the presented work, this matrix burner is not directly resolved. Instead, a corresponding, cylindrically shaped area according to the matrix burner outlet section is subject to stochastic, time-correlated forcing for temperature and velocity. This forcing approach realizes turbulent decay in time. Spatial decorrelation of the turbulent signals due to shear effects is neglected in the forcing due to the very low bulk velocity of $\bar{U}_{cf} = 2.5\ m/s$. Time-coherent, stochastic forcing is realized with a first order Langevin equation (Pope, 2000), reading

$$\Phi(t+\Delta t) = \Phi(t) - {\Phi(t)\Delta t}/{\tau_T} + \sqrt{2\sigma^2\Delta t/\tau_T}\,\xi(t). \quad (2)$$

Here, $\Phi \in [T, U_{cf}]$ and τ_T denotes the upstream integral turbulent time-scale, which is predefined by measurements (Rodrigues et al., 2015). σ is the standard deviation of the process and $\xi(t)$ is a random forcing with Gaussian distribution, which is independent of Φ and fulfils the properties

$$\langle\xi(t)\rangle = 0,\quad \langle\xi(t)^2\rangle = 1,\quad \langle\xi(t)\xi(t')\rangle = 0,\quad t \neq t'. \quad (3)$$

Equation (2) therefore realizes an ergodic, statistically stationary Ornstein-Uhlenbeck process. Its properties are depicted for an exemplary signal in Fig. 5.

The stochastic forcing, applied for temperature and

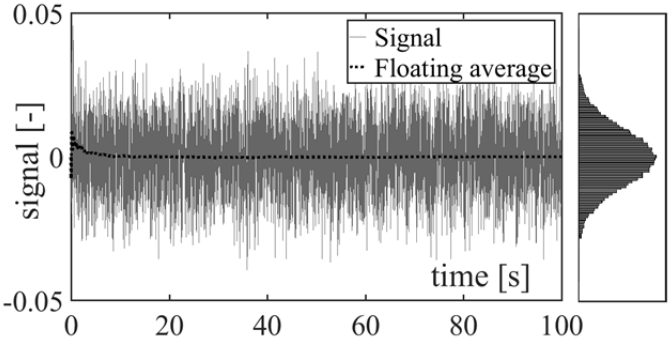

Figure 5 Exemplary upstream forcing signal from the Langevin approach.

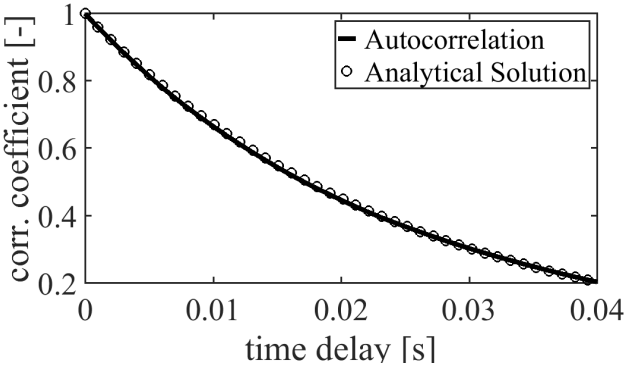

Figure 6 Analytical correlation for upstream forcing signal and numerical realization.

velocity fluctuations, as induced by the upstream matrix burner, generates correlated noise. The inherent turbulence induced decay can be described by the analytical solution of Eq. (2), which reads $R_0 = \exp(-\tau/\tau_s)$. Numerical forcing and analytical solution are compared in Fig. 6. The comparison of analytical and numerical correlation function in Fig. 6 shows that upstream numerically forced temperature and velocity fluctuations almost exactly follow the properties of the Langevin equation, Eq. (2). The forced signals spectra energy content, which is consecutively convected to the reaction zone, is shown in Fig. 7. Therefrom it is evident that the presented stochastic forcing approach realizes a $1/f$-like spectral shape, as induced similarly by turbulent fluctuations.

Since stochastic forcing is applied at mass flow inlet boundary conditions only, there should be no model induced decay downstream and turbulent structures are supposed to be convected to the reaction zone as frozen structures, as can be expressed by

$$\begin{aligned} DT'/Dt &= 0, \\ Du'/Dt &= 0, \end{aligned} \tag{4}$$

with $D/Dt = \partial/\partial t + \bar{U}_{cf} \cdot \nabla$. However, the convected temperature spots and velocity perturbations are subject to artificial decay as they are transported along the pre-atomizer region. This is indicated by cross-correlation of temperature fluctuations, shown in Fig. 8.

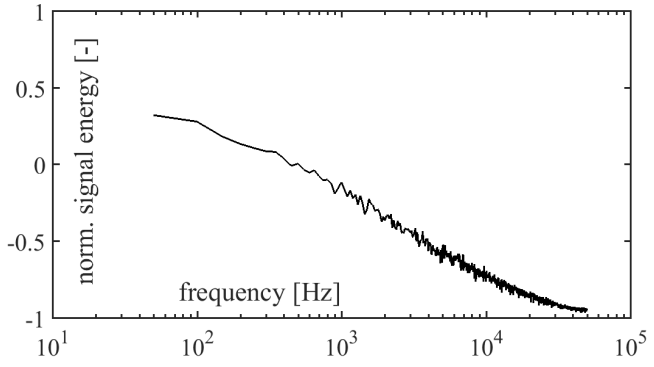

Figure 7 Spectral distribution of energy content of the upstream forcing signals.

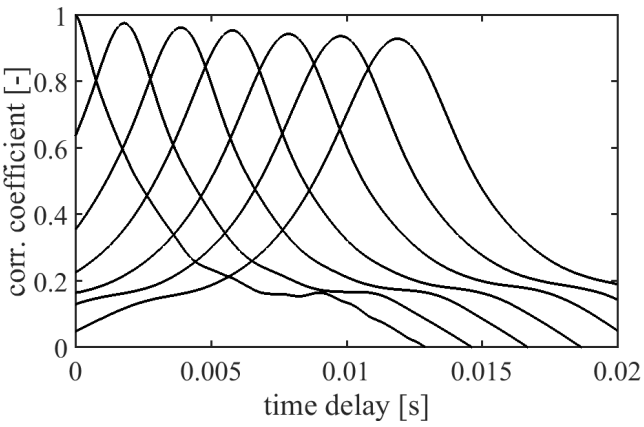

Figure 8 Cross-correlation of downstream fluctuating temperature signals after stochastic forcing.

Cross-correlation in Fig. 8 is carried out on seven monitor points on an exemplary streamline in the co-flow section of the burner. About 20000 discrete data points are taken into consideration, respectively, with a monitoring point distance along the streamline of $\Delta x = 0.0045m$. The constant separation time of downstream correlation peaks is due to a constant convection velocity of $\bar{U}_{cf} = 2.5\, m/s$. Downstream correlation functions are slightly wider compared to upstream distributions. This is expected to be due to rather large scale fluctuations and shear effects. The artificially induced decay, as expressed by downstream Gaussian peaks not reaching a correlation value of one, are expected to be due to numerical dissipation.

RESULTS AND DISCUSSION

For comparison with the experimental data, simulation results from the liquid and dispersed phase are averaged circumferentially during post processing. However, since asymmetries exist in the experimental data the simulations are compared with the full radial data. In the LES over 80% of the turbulent kinetic energy are resolved indicating a well resolved LES.

Validation of Spray Boundary Condition

Comparison between experimental and computed radial profiles of SMD at different heights above the atomizer is displayed in Fig. 9. Simulation data is taken from the LES case. The trend and magnitude of droplet SMD in the simulation is in good agreement with the measurements except for the inner region of the spray where the LES predicts a strong decline in droplet mean diameter which is not present in the experiment. This could be due to an overestimation of evaporation rate by the model or the fact that droplet size in the boundary condition is not conditioned on the injection angle. Therefore, too many small droplets are present in the inner region. However, based on the results it is concluded that the spray boundary condition as described in the previous section is a valid representation of the actual atomizer.

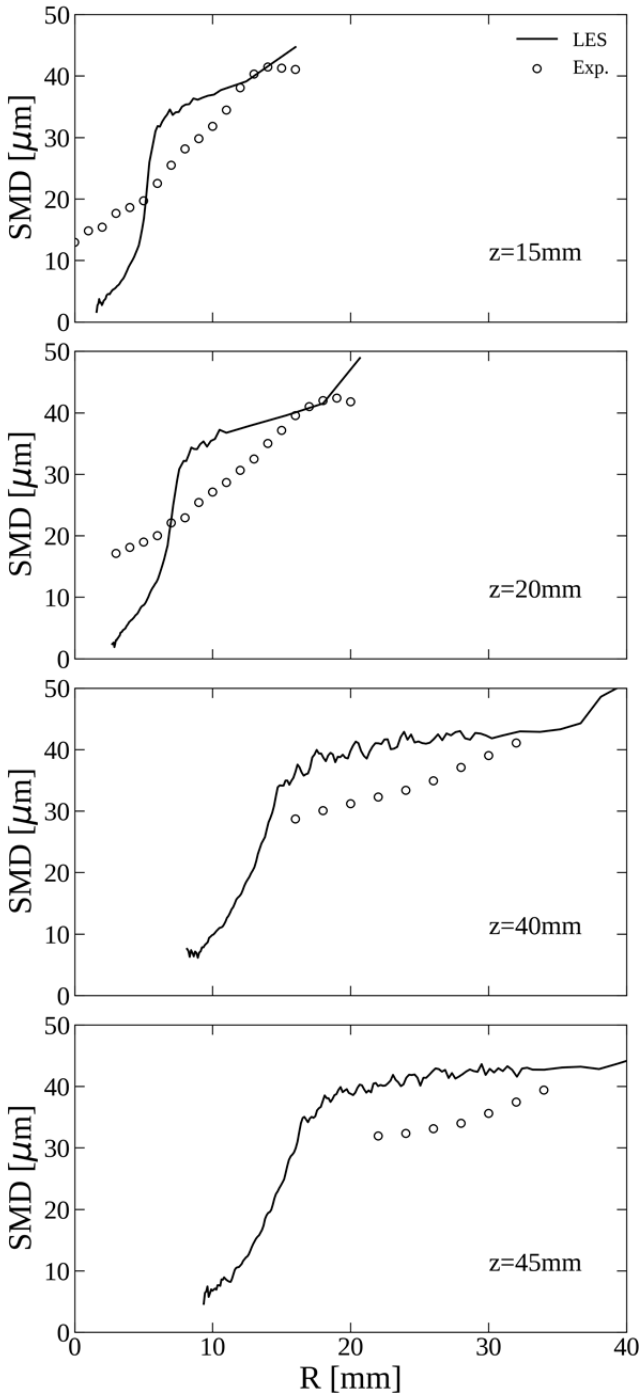

Figure 9 Radial profiles of SMD at different axial locations.

Although not shown here, the URANS and SAS both show the same general tendencies in the liquid phase as the LES.

Gas phase results

Time averaged contour of temperature in the $x = 0mm$ plane from the LES is given in Fig. 10. The flame is clearly lifted above the spray cone which is consistent with the behaviour in the experiment as shown in Fig. 2. Gas temperature drops considerably below the co-flow

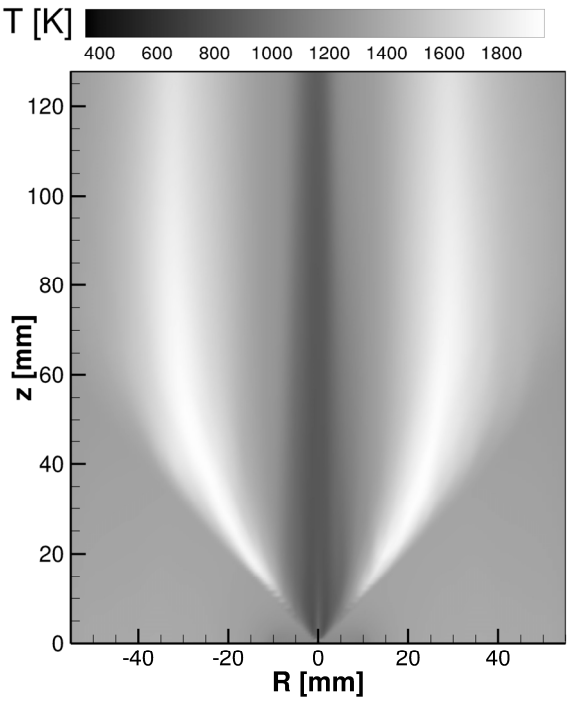

Figure 10 Contour of mean temperature in a mid-plane cut from LES.

temperature in the centreline region due to high evaporation rates and cooling from the small droplets which are trapped in the inner region (see Fig. 9).

Data from radial temperature profiles in Fig. 11 demonstrates excellent agreement of all simulations with the experiment up to an axial distance of $z = 40mm$. Peak temperature magnitude and position are precisely met. As evident from the radial displacement of peak temperature at $z = 60mm$, the simulations tend to overpredict the spreading rate of the flame at higher elevations. A similar behaviour has been reported in other studies (Ma et al, 2016b; Gallot-Lavallée, 2017).

Comparing the different simulation methods, the URANS predicts a slightly higher maximum temperature in the profile at $z = 15mm$ than the other simulations. Furthermore, a bump in the inner flame front exists in the URANS for all profiles which is not present in the other simulations and the experiments. It should be pointed out that the URANS based on the coarse grid provides similar accuracy to the URANS on the standard grid indicating a sufficient grid resolution even on the coarse grid. Apart from that, all simulations compute very similar results for mean temperature.

Results for Root Mean Square (RMS) temperature fluctuations are given in Fig. 12. For the URANS, fluctuations are modelled using Eq. (1) while from the SAS and LES resolved fluctuations are presented. As evident from the plots, the considerable high background level of fluctuations is met by all simulations over the region of interest. In the URANS this is achieved by the transport of the specified inflow fluctuation for Eq. (1). For the SAS and

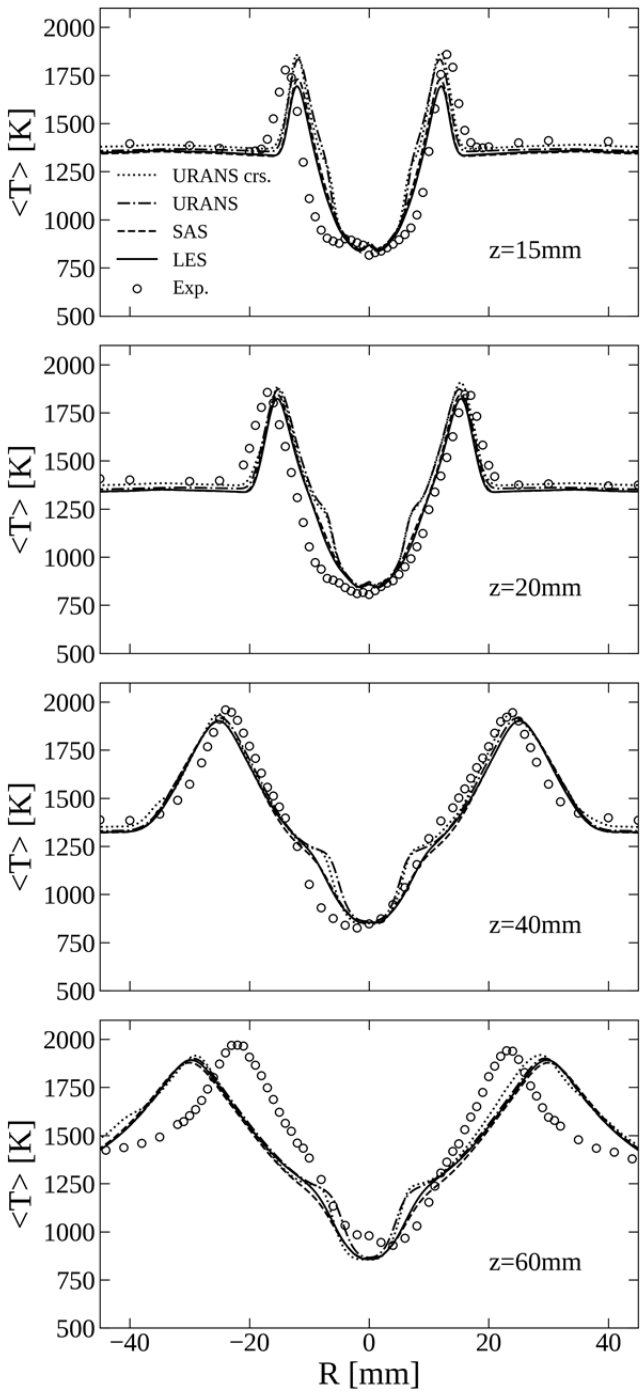

Figure 11 Radial profiles of gas temperature at different axial locations.

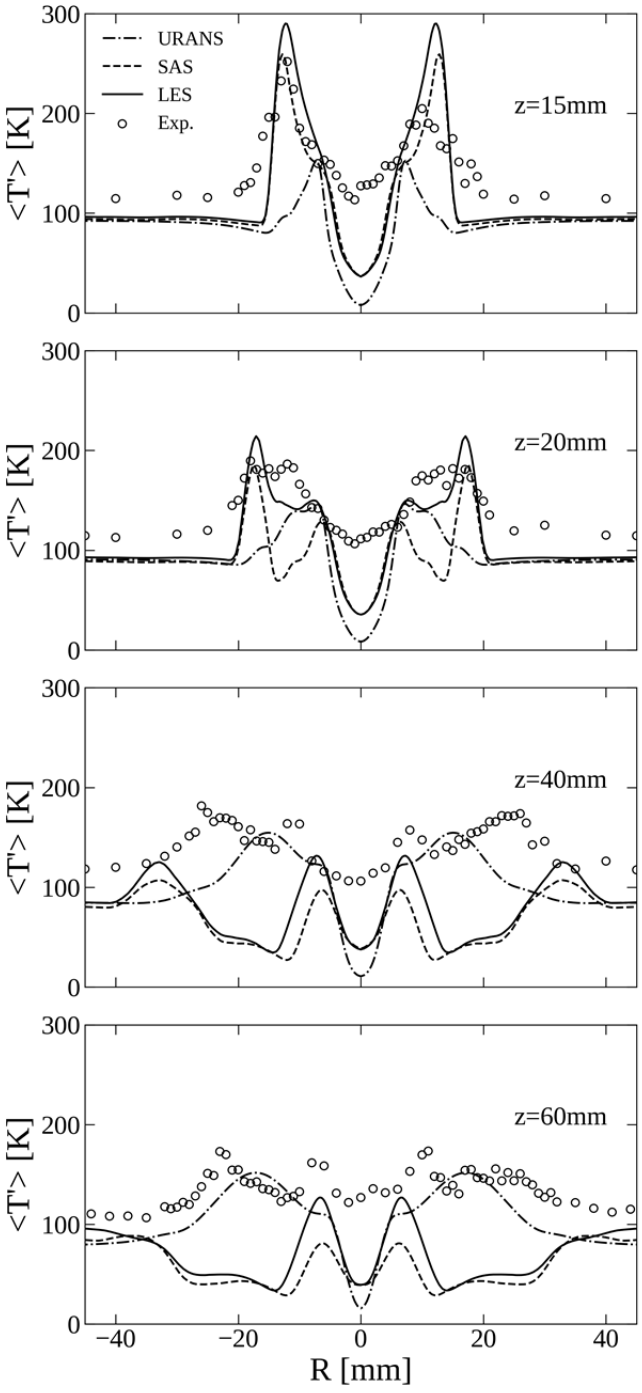

Figure 12 Radial profiles of RMS temperature fluctuation at different axial locations.

LES the stochastic Langevin process at the inlet is able to realize the background level produced by the upstream matrix burner.

At the $z = 15mm$ measurement position the peaks in fluctuation at the flame edge are reproduced by the SAS and LES, whereas the URANS stays at a considerable lower maximum level. With increasing axial distance from the atomizer, differences between SAS and LES become more evident as lower fluctuation intensities are replicated in the SAS. This could indicate that the SAS is not fully switched to the LES mode in this region. As a consequence, fluctuations are damped by the modelled turbulent viscosity. At $z = 40mm$ and $z = 60mm$ the LES matches the general trend of fluctuations with two characteristic peaks but underestimates the magnitude in the flame region. At these elevations the modelled fluctuation intensity from the URANS agrees better with the experiment. In contrast to the experimental data, a distinct drop in temperature RMS along the centerline (R=0mm) is evident in all simulation cases.

Keeping in mind that the fluctuations in the URANS require additional modelling and therefore additional input, the scale resolving simulations and especially the LES perform better in terms of temperature fluctuations.

CONCLUSIONS

Numerical simulations of the Delft Spray in Hot Co-Flow flame HII were carried out using simulation methods of different fidelity. Special emphasis was put on the description of inflow turbulent velocity and temperature fluctuations due to their vast influence on the accurate representation of the flame. Therefore, a first order Langevin signal was imposed on the mean quantities of the inflow. The consistency of this approach was verified by means of an analytical solution and energy spectra which showed a $1/f$-like spectral shape, as induced similarly by turbulent fluctuations.

Simulations results indicated an over representation of small droplets in the inner flame region as a result of the used spray boundary condition. Nevertheless, radial profiles of mean temperature showed excellent agreement with measurement data for all simulation approaches. Highest deviation was identified for the URANS. Thus, all three simulation methods were able to capture the general features of the MILD flame in the case considered. Regarding temperature RMS fluctuations, the scale resolving simulations using the inlet forcing signal were able to provide better results than the model used in the URANS although fluctuations were subject to damping for the far downstream measurement positions.

Therefore, it is concluded that the upstream flow and temperature forcing as introduced in the present work is able to provide a consistent inflow signal in case of low Reynolds number flows such as the DSHC flame.

Furthermore, the used simulation framework is able to reproduce multiphase combustion under MILD condition and can therefore offer detailed insight into the combustion process of industrial scale applications, too.

However, special emphasis should be put on the influence of spray boundary conditions on the simulation in further studies.

NOMENCLATURE

Abbreviations

A-PDF	Assumed Probability Density Function	-
CARS	Coherent Anti-Stokes Raman Spectroscopy	-
CDS	Central Differencing Scheme	-
crs	Coarse	-
DLR	German Aerospace Center	-
DNG	Durch Natural Gas	-
DSHC	Delft Spray in Hot Co-flow	-
FRC	Finite Rate Chemistry	-
QUDS	Quadratic Upwind Differencing Scheme	-
LDA	Laser Doppler Anemometry	-
LES	Large Eddy Simulation	-
MILD	Moderate or Low-Oxygen Dilution	-
PDA	Phase Doppler Anemometry	-
URANS	Unsteady RANS	-
RANS	Reynolds Averaged Navier Stokes	-
TCI	Turbulence Chemistry Interaction	-
THETA	Turbulent Heat Release Extension for the Tau Code	-
TPB	Three Point Backward	-
SAS	Scale Adaptive Simulation	-
SMD	Sauter Mean Diameter	m
SST	Shear Stress Transport	-

Dimensionless Numbers

Pr	Prandtl number	-
Re	Reynolds number	-
We	Weber number	-

Variables (Latin)

D	Diameter, computational domain	m
H	Height, computational domain	m
h	Measurement height	m
$\dot{m}$	Mass flow rate	kg/s
p	Pressure	Pa
T	Temperature	K
$\widetilde{T''^2}$	Temperature standard deviation	K^2
t	Time	s
U, u	Velocity	m/s
X	Molecule mass fraction	$-$
x, y, z	Spatial coordinates	m

Variables (Greek)

Δ	Delta	-
$\nabla, \nabla\cdot$	Gradient, Divergence	-
μ, μ_t	Viscosity (dynamic), turbulent	
ξ	White noise, Gaussian	-
ϱ	Density	kg/m^3
σ	Standard deviation	K^2
τ	Time	s
τ_T	Turbulent time-scale	s
Φ	Variable	-

ACKNOWLEDGMENTS

The authors would like to thank Prof. D.M. Roekarts for providing the experimental database on the DSHC flame.

REFERENCES

[1] Cavaliere, A., and Joannon M. (2004) "Mild combustion." Progress in Energy and Combustion science 30.4: 329-366.

[2] De Joannon, M., et al. (2005) "Analysis of process parameters for steady operations in methane mild combustion technology." Proceedings of the Combustion Institute 30.2: 2605-2612.

[3] Mancini, M., et al. (2007) "On mathematical modelling of flameless combustion." Combustion and flame 150.1: 54-59.

[4] Li, P., et al. (2014) "MILD combustion under different premixing patterns and characteristics of the reaction regime." Energy & Fuels 28.3: 2211-2226.

[5] Ye J., et al. (2015). An experimental study on MILD combustion of prevaporised liquid fuels, Appl. Energy 151, 93-101. DOI: 10.1016/j.apenergy.2015.04.019

[9] Reddy, V. Mahendra, et al. (2015) "Experimental and numerical analysis for high intensity swirl based ultra-low emission flameless combustor operating with liquid fuels." Proceedings of the Combustion Institute 35: 3581-3589.

[10] Weber R., Smart J.P., and Kamp W.V. (2005). On the (MILD) combustion of gaseous, liquid, and solid fuels in high temperature preheated air, Proc. Combust. Inst. 30 (2), 2623-2629. DOI: 10.1016/j.proci.2004.08.101

[11] Rodrigues H.C., Tummers M.J., van Veen E.H., and Roekaerts D.J.E.M. (2015). Spray flame structure in conventional and hot-diluted combustion regime, Combustion and Flame 162, 759-773. DOI: 10.1016/j.combustflame.2014.07.033

[12] Ma, Likun, et al (2016a). "Transported PDF modeling of ethanol spray in hot-diluted coflow flame." Flow, Turbulence and Combustion 96.2: 469-502.

[13] Ma L., et al (2016b). Numerical investigation of ethanol spray-in-hot coflow flame using steady flamelet model, Combust. Flame 162, 759-773.

[14] Gallot-Lavallée, S., et al (2017). "Large Eddy Simulation of an ethanol spray flame under MILD combustion with the stochastic fields method." Proceedings of the Combustion Institute 36.2: 2577-2584.

[15] Menter, Florian, et al (2003). "A scale-adaptive simulation model for turbulent flow predictions." 41st aerospace sciences meeting and exhibit.

[16] Klein, M., et al. (2003) "A digital filter based generation of inflow data for spatially developing direct numerical or large eddy simulations." Journal of Computational Physics 186.2: 652-665.

[17] Ma L. and Roekaerts D. (2016). Structure of spray in hot-diluted coflow flames under different coflow conditions: A numerical study, Combustion and Flame 172, 20-37. DOI: 10.1016/j.combustflame.2016.06.017

[18] Domenico M.D., Gerlinger P., and Noll, B. (2011). Numerical Simulations of Confined, Turbulent, Lean, Premixed Flames using a Detailed Chemistry Combustion Model. In: Proceedings of the ASME Turbo Expo 2011 – GT2011-45520.

[19] Reichling G., Noll B., and Aigner M. (2013). Development of a Projection-Based Method for the Numerical Calculation of Compressible Reactive Flows. In: Proceedings of the 51st AIAA Aerospace Sciences Meeting – AIAA2013-2434.

[20] Eckel, Georg, et al. (2016) "Semi-empirical model for the unsteady shear breakup of liquid jets in cross-flow." Atomization and Sprays 26.7

[21] Pope S.B. (2000). Turbulent Flows. Cambridge, UK: Cambridge University Press. ISBN 0-521-59886-9.

[22] Röhl, Olaf, and Norbert Peters. (2009) "A reduced mechanism for ethanol oxidation." 4th European Combustion Meeting (ECM 2009), Vienna, Austria, April.

[23] Lefebvre, Arthur H. (1998). Gas turbine combustion. CRC press,

[24] Abramzon, B., and W. A. Sirignano. (1989). "Droplet vaporization model for spray combustion calculations." International journal of heat and mass transfer 32.9: 1605-1618.

[25] Gosman, A. D., and E. Loannides. (1983) "Aspects of computer simulation of liquid-fueled combustors." Journal of Energy 7.6: 482-490.

[26] Bini, M., and W. P. Jones (2008). "Large-eddy simulation of particle-laden turbulent flows." Journal of Fluid Mechanics 614: 207-252.